IEEE Access
Multidisciplinary | Rapid Review | Open Access Journal

Received 5 April 2024, accepted 26 April 2024, date of publication 30 April 2024, date of current version 9 May 2024.

Digital Object Identifier 10.1109/ACCESS.2024.3395451

APPLIED RESEARCH

A Novel Voltage–Current Dual-Drop Control Method for Shipboard DC Micro-Grid With Energy Storage Systems

XUN CHEN[1], (Member, IEEE), RUI TIAN[1], (Student Member, IEEE), SONG XU[1], (Member, IEEE), WEI JIANG[2], (Member, IEEE), YONGHONG WANG[3], (Student Member, IEEE), AND SEIJI HASHIMOTO[4], (Member, IEEE)

[1]School of Automation, Jiangsu University of Science and Technology, Zhenjiang, Jiangsu 212100, China
[2]College of Intelligent Manufacturing, Yangzhou Polytechnic Institute, Yangzhou, Jiangsu 215126, China
[3]Department of Electronic Information Teaching, Guangzhou Information Technology Vocational School, Guangzhou 510515, China
[4]Department of Electronics and Informatics, Gunma University, Kiryu, Gunma 376-8515, Japan

Corresponding author: Song Xu (songxu@just.edu.cn)

This work was supported by the Natural Science Foundation of Jiangsu University of Science and Technology under Grant 1032932101.

ABSTRACT The DC micro-grid system, as a new generation of shipboard DC micro-grid system, has the advantages of integrating renewable energy and enhancing the stability and reliability of the power system. For the energy distribution problem of energy storage battery charging and discharging in shipboard DC micro-grid, P-V voltage droop control and SOC-I current droop control methods are proposed. The SOC-I control method incorporated in the battery charging and discharging process can effectively balance the SOC and output power of the energy storage battery. For the on/off-grid process of shipboard power converter and onshore power, the control method of voltage and current control mode switching is proposed, which realizes the fast response of output voltage in off-grid mode and the controllable transfer of power interacting with the grid in grid-connected mode. Secondly, a pre-synchronized control based on amplitude and frequency modulation achieves a flexible on-grid/off-grid connection of the power converter. A method based on the parallel connection of multiple reduced-order generalized integrator (ROGI) is introduced to achieve suppression of output voltage unbalance as well as 5*th* and 7*th* harmonics. Finally, the efficiency and correctness of the proposed control method has been successfully evaluated an level 750KVA shipboard micro-grid system.

INDEX TERMS Energy storage converter, harmonic suppression, on/off-grid control, shipboard DC micro-grid system, voltage-current dual-droop control.

I. INTRODUCTION

Over the past few decades, shipboard power distribution systems were mostly based on conventional AC grids. However, with the development of power electronics as well as energy storage and other technologies, the advantages of DC micro-grid systems have gradually emerged. The transmission technology of conventional DC micro-grid is more mature, and the reliability of grid operation is high. It also reduces the power of electronic conversion devices, which reduces the loss of energy conversion. DC micro-grid system can be isolated into a small power system, so it has a high degree of flexibility. It can be applied to islands or ships and other scenarios with isolated characteristics. Although the ship micro-grid system has obvious advantages compared with the traditional ship AC power grid, because of its isolated characteristics and mobile characteristics, the environment is more severe compared with the conventional DC micro-grid facing more complex working conditions [1].

Conventional DC micro-grid systems are usually applied on land and are, therefore, larger in terms of power capacity. The power capacity of the ship micro-grid system is limited

The associate editor coordinating the review of this manuscript and approving it for publication was Zhilei Yao.

© 2024 The Authors. This work is licensed under a Creative Commons Attribution-NonCommercial-NoDerivatives 4.0 License.
For more information, see https://creativecommons.org/licenses/by-nc-nd/4.0/

by the size of the ship, so when the system is disturbed, the bus voltage is more likely to fluctuate, which leads to power fluctuations in the ship DC micro-grid. When the ship is running at sea, the external environment is extremely complex, so it is necessary to distribute reasonably for each unit in the shipboard DC micro-grid system. Micro-grid system. To improve the stability of ship DC micro-grid, energy storage systems are often introduced into the micro-grid system to smooth out power fluctuations [2], [3], [4]. As an important device connecting the energy storage unit and the DC bus, the energy storage converter can realize the functions of charging and discharging management of the energy storage unit and grid scheduling, which can directly affect the stability of the DC micro-grid system operation.

The energy storage converter is an indispensable link for realizing the two-way interaction of energy between the DC bus and the energy storage device, so the research on the control strategy of its charging and discharging process is crucial [5]. Bidirectional energy storage converter belongs to the power conversion device, the basic control strategy of the power conversion device includes: constant power control (P/Q control) [6], constant frequency and constant voltage control (V/F control) [7], and droop control [8]. When the energy storage converter works in the P/Q control mode, it is in the current source state, intending to control the current output by the converter [9], [10], [11]. Generally, when the grid-connected operation of the micro-grid (shipboard DC micro-grid and shore power grid similar to the grid-connected operation of the micro-grid) has a main power supply, the energy storage converter will choose to use the P/Q control with the energy management system to achieve the micro-grid and the main grid between the exchange of power [12], [13], [14]. The storage converter operates in the V/F mode in the voltage source state, and the storage converter can be selected to operate in the V/F control mode when a loss of power from the mains supply requires the storage converter to establish and maintain system AC voltage and frequency stability [15], [16]. The droop control application is more flexible and can work both in the grid-connected state and the off-grid state. The converters in islanded operating micro-grid (such as shipboard DC micro-grid during normal navigation) typically employ V/F control and droop control [17], [18]. However, V/F control is predominantly utilized for single working converters [19]. Droop control, on the other hand, is extensively employed in parallel operation converters due to its ability to facilitate interconnection-free power distribution between parallel converters. This is particularly advantageous during mode conversion between shipboard DC micro-grid and shore power grid, where the adoption of droop control not only enhances the success rate of conversion but also enables a seamless transition [20].

At present, the research and application of domestic and foreign scholars for converter on/off-grid flexible switching, power transfer control, and other technologies are mainly focused on the fields of uninterruptible power supply, distributed grid, micro-grid, and new energy generation. References [21] and [22] adopt adaptive droop control and virtual synchronous generator methods, respectively, but due to the variability of power supply capacity and frequency of the grid, its regulation ability is limited, and the power transfer and precise control effect are not good. The unified control mode using voltage outer loop and current inner loop does not require control mode switching, thus it is easy to realize smooth switching between on/off-grid, but the dynamic response of the power supply converter, which is controlled as a current source characteristic in the off-grid mode, is slow, and the disadvantage is especially obvious in the occasion of load high-power casting and switching. Reference [23] gives a seamless switching control method for battery storage inverters and diesel generators, which requires the addition of an upper-level control unit in addition to the local controller to realize the coordinated control of the two, increasing the complexity of the control system. Reference [24] introduces an improved phase-locked loop that does not rely on the fastness of islanded detection and does not require an additional pre-synchronization process but suffers from the shortcomings of a wide range of fluctuations in output voltage magnitude and frequency. Reference [25] requires the prediction of the regulator's output state or considers the current reference to remain unchanged before and after the control mode switching to avoid large oscillations and overshooting of the regulator and current during the switching process, but it cannot be adapted to the working conditions where there are step changes in the load or output power during the switching process.

In shipboard DC micro-grid system, harmonics can affect the control accuracy of the ship's system and increase the overall energy consumption of the ship. To solve the harmonic problem, active suppression is achieved by improving the source, and passive suppression is achieved by adding additional filtering equipment. Considering the limited space of the ship, the active suppression scheme is used to investigate the rectifier. References [26] and [27] improve the rectifier topology, while reference [28] innovate the modulation method of the rectifier to realize the reduction of harmonic distortion. The passive suppression strategy requires the addition of additional filtering equipment, so the active suppression strategy is used to suppress harmonics at the control level of the power generation system. References [29] and [30] mention the use of second-order generalized integrators for harmonic extraction. Reference [31] demonstrates that the use of SOGI can lead to a 30% reduction in total harmonic distortion. Reference [32] mentions a reduced-order generalized integrator developed on SOGI; compared to SOGI, ROGI can be designed more flexibly for specified harmonic compensation, with half the computational effort of SOGI [33].

Existing control methods for energy storage converter charging/discharging control and power supply converter on/off-grid control. It will be limited by the variability of the grid power supply capacity and frequency, resulting in limited regulation capability and poor power transfer and precise

control. The harmonic problem of the output voltage of the power supply converter will affect the control accuracy of the ship system and increase the overall energy consumption of the ship. Therefore, a converter control method based on voltage-current control is proposed. The control strategy effectively solves the energy distribution of the energy storage converter during operation and the SOC equalization of the storage battery, and stabilizes the DC bus voltage. Flexible on/off-grid control is realized to ensure the fast response of output voltage in off-grid mode and the controllable transfer of power interacting with the grid in grid-connected mode, as well as the suppression of harmonic problems of output voltage.

The paper is organized as follows. Section II describes the composition of the shipboard DC micro-grid system, the energy storage converter, and the overall control strategy of the power supply converter. Section III introduces the charging/discharging control strategy of the energy storage converter, the on/off-grid control strategy of the power supply converter and the AC shore power, the pre-synchronization control strategy of the shore power, and the harmonic suppression control strategy of the output voltage of the power supply converter. Section IV builds the experimental platform and validates the proposed control strategies. Finally, Section V summarizes this study.

II. SHIPBOARD DC MICRO-GRID SYSTEM

A. TOPOLOGICAL STRUCTURE

The topology of the shipboard DC micro-grid system is shown in Fig. 1, which is divided into two subsystems, the port-side DC micro-grid and the starboard-side DC micro-grid.

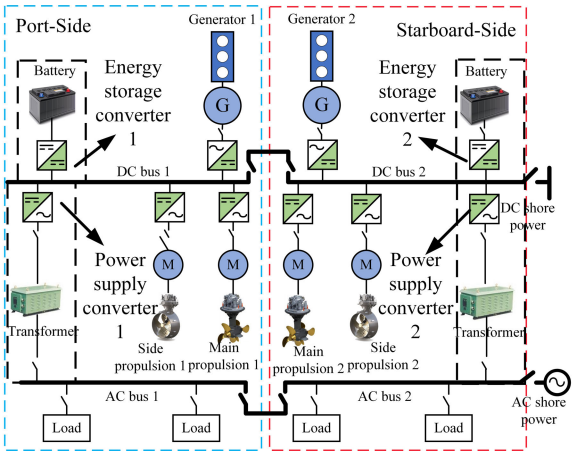

FIGURE 1. Topology of shipboard DC micro-grid system.

Each subsystem comprises an energy storage converter, generator rectifier, propulsion motor converter, and load supply converter. The DC side of each subsystem utilizes the DC bus as a common connection point. DC bus 1 and DC bus 2 can operate either in a network or independently through circuit breakers. Similarly, AC bus 1 and AC bus 2 can be networked or operated independently through circuit breakers. Furthermore, the ship can establish connections to the DC shore power grid through DC bus 2 or to the AC shore power grid through AC bus 2, enabling uninterrupted power supply while the ship is docked. This dual connectivity enhances flexibility in power management. To cater to the dynamic energy requirements of the ship, the energy storage converter possesses the capability to seamlessly switch between charge and discharge modes based on real-time conditions. This adaptability ensures optimal energy utilization and contributes to the overall efficiency of the ship's power system.

B. ENERGY STORAGE CONVERTER CONTROL STRATEGY

The overall control block diagram of the energy storage converter charging and discharging is shown in Fig. 2. In the actual charging process, to realize fast charging and prolong the service life of the energy storage battery while avoiding overcharging and overcurrent phenomenon, the combination of the three stages of the ''constant current - constant voltage - float charging'' charging method is usually adopted. Among them, float charging is used to compensate for the self-discharge of the energy storage unit, and its control structure is the same as that of the constant voltage stage. In the energy storage system in this paper, the two-stage charging method of ''constant current-constant voltage'' is adopted. A dual closed-loop control strategy is adopted, and a segmented charging mode is used to avoid overcharging or overcurrent during the charging process.

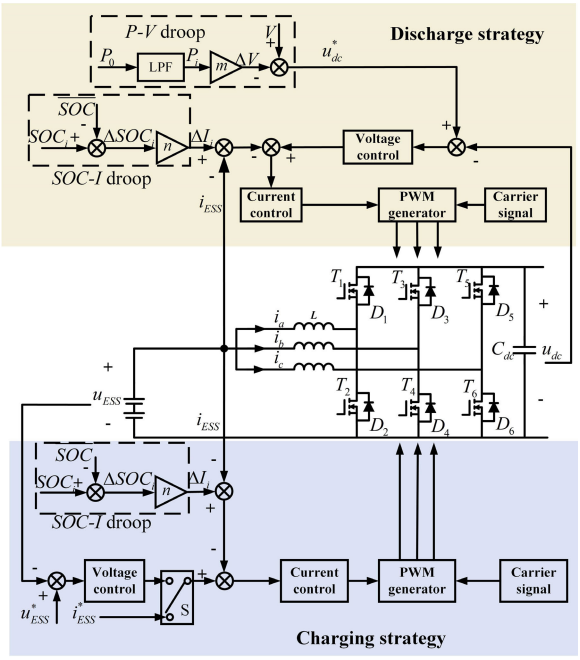

FIGURE 2. Energy storage converter control block diagram.

During the discharge process of the energy storage unit, the DC bus voltage is stabilized to ensure the stability of the DC network system. A dual droop control strategy for P-V voltage and SOC-I current is introduced. When multiple

energy storage converters are operated in parallel, P-V droop control is used in the voltage loop to realize the distribution of the output power of multiple converters according to the ratio of their respective capacities, and SOC-I droop control is introduced in the current loop to ensure the equalization of the SOC state of the storage battery packs corresponding to the energy storage converters during the operation process.

C. POWER SUPPLY CONVERTER CONTROL STRATEGY

The shipboard power converter is connected from the DC bus and passes through a transformer to supply the shipboard AC loads. There are three operating modes for the normal operation of the shipboard power supply converter: off-grid mode, grid-connected mode, and pre-synchronized mode. In off-grid mode, the power supply converter can be divided into parallel operation and independent operation. In parallel operation, droop control is adopted; in independent operation, constant voltage/frequency control is adopted. In grid-connected mode, the port side power supply converter or the starboard side power supply converter is operated independently in parallel with the shore power, and the power transfer from the grid-connected power supply converter to the shore power is withdrawn from operation. Pre-synchronization control is required before grid connection to avoid instantaneous voltage shocks. Simultaneously, multiple ROGI output voltage harmonic suppression methods are introduced to ensure voltage stability during on/off-grid connection. Its overall control block diagram is shown in Fig.3.

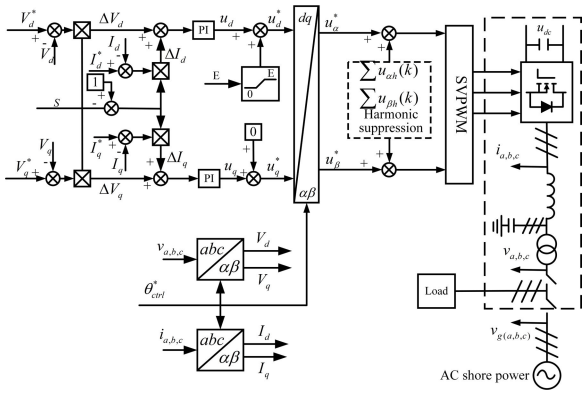

FIGURE 3. Supply converter control block diagram.

III. SHIPBOARD CONVERTER CONTROL METHOD

A. ENERGY STORAGE CONVERTER CHARGING CONTROL

The two-stage charging control principle of the energy storage battery is illustrated by Fig. 4. A dual closed-loop control strategy with a segmented charging mode is used to avoid overcharging or overcurrent during the charging process. In the initial charging stage, the energy storage converter undergoes constant current charging, with the voltage outer loop not involved in control. The current reference is set to a constant value, denoted as i^*_{ESS}. Consequently, the terminal voltage of the energy storage unit gradually increases. When the terminal voltage reaches the

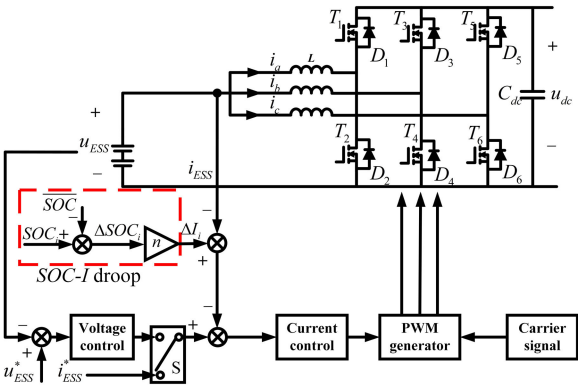

FIGURE 4. Charging control principle block diagram.

predefined set value, the energy storage converter transitions to constant voltage charging. During this phase, the voltage outer loop becomes active, operating in conjunction with the current inner loop. The voltage reference value u^*_{ESS} is held constant and is controlled in a closed loop by providing feedback from the terminal voltage of the energy storage battery. Throughout the charging process, the current reference value switches from a constant value to the output value of the voltage loop.

According to the topology of the energy storage converter, the constant-current charging equation of the energy storage battery can be obtained with the charging current i_{ess} as the state variable:

$$L\frac{di_{ESS}(t)}{dt} = u_{ESS} - Du_{dc} \tag{1}$$

From (1), the control equation of the current loop can be obtained as:

$$D = \frac{(k_p + \frac{k_i}{s})(i^*_{ESS} - i_{ESS}) + u_{ESS}}{u_{dc}} \tag{2}$$

where D is the duty cycle of the control circuit, and k_p and k_s are the proportional coefficients of the PI controller.

To effectively control the battery charging state and prevent overcharging, the SOC-I droop control strategy is introduced into the current loop. In this strategy, the SOC value of each energy storage battery differs from the average value, and this difference is amplified by the proportional unit. Subsequently, it is superimposed into the current command, thereby modifying the magnitude of the battery charging current.

B. ENERGY STORAGE CONVERTER DISCHARGE CONTROL

The block diagram illustrating the energy storage converter discharge control principle is presented in Fig. 5. P-V droop control is added to the voltage outer loop to stabilize the bus voltage by adjusting the active power of the converter. The active power P_0 output from the converter to the DC bus is low-pass filtered and multiplied by the droop coefficient m. The reference value u^*_{dc} of the DC bus voltage is calculated and fed back to the DC bus voltage for voltage closed-loop control. Batteries with different initial SOC provide different

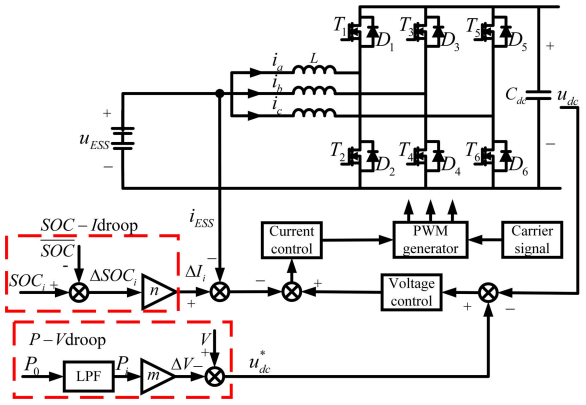

FIGURE 5. Discharge control block diagram.

amounts of energy when they start discharging, which may lead to the fact that some batteries reach the lowest SOC first in the discharging phase, while others still have more energy available for release, which may lead to the unbalanced performance of the system, affecting the stable operation of the system, and therefore a SOC-I droop control strategy is added to the current inner loop. The current closed-loop control is carried out by feeding back the battery discharge current by taking the difference between the SOC of each storage battery and the average value of the SOC of the storage battery through the proportional link, and the equalization control of the battery SOC state is achieved by changing the size of the discharge current of the storage battery.

1) P-V DROP CONTROL

In this paper, voltage and current dual-drop control is used as the control method of the energy storage converter. The equivalent circuit of the ship power supply and converter connected to the bus can be simplified in Fig. 6.

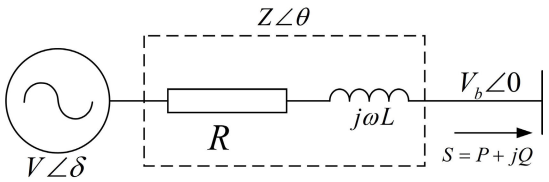

FIGURE 6. Schematic diagram of ship power energy transmission.

In Fig. 6, $V_b\angle 0$ is the common bus voltage, $V\angle\delta$ is the output voltage of the ship's power supply, V is the voltage magnitude, δ is the voltage power angle, $Z\angle\theta = R + j\omega L$ is the equivalent impedance of the ship's power supply, S is the apparent power of the ship's power supply, P is the output active power, and Q is the output reactive power, which can be expressed as:

$$\begin{aligned} P &= \left(\frac{V_b V}{Z}cos\delta - \frac{V_b^2}{Z}\right)cos\theta + \frac{V_b V}{Z}sin\delta sin\theta \\ Q &= \left(\frac{V_b V}{Z}cos\delta - \frac{V_b^2}{Z}\right)sin\theta - \frac{V_b V}{Z}sin\delta cos\theta \end{aligned} \tag{3}$$

Usually, the voltage power angle difference δ between the output of the power supply and the bus is very small, i.e., $sin\delta \approx \delta$, $cos\delta \approx 1$. The energy storage lines of the shipboard DC micro-grid are resistive and thus can be equated to a purely resistive impedance, and P and Q under pure resistivity can be expressed as follows:

$$\begin{aligned} P &\approx \frac{V_b(V - V_b)}{R} \\ Q &\approx -\frac{V_b V}{R}\delta \end{aligned} \tag{4}$$

The interdependence of active power and voltage is evident from (4). Fig. 7 illustrates the resistive impedance P-V droop characteristic curve, demonstrating that voltage can be modulated by manipulating active power.

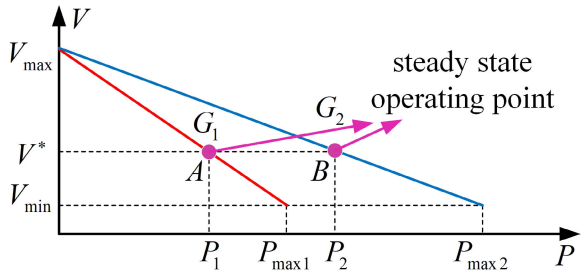

FIGURE 7. Schematic diagram of P-V droop curve.

G1 and G2 shown in Fig. 7 represent the port energy storage converter and the starboard energy storage converter. The droop control curve equation of each converter is as follows:

$$\begin{aligned} V_i^* &= V_{max} - m_i \cdot P_i \\ m_i &= \frac{V_{max} - V_{min}}{P_{maxi}} \end{aligned} \tag{5}$$

where i represents the number of the parallel converter ($i = 1, 2$), and m_i represents the droop coefficient of the converter. V_i^* represents the reference value of the DC voltage, V_{max} represents the maximum operating voltage allowed when the converter is connected in parallel, and V_{min} represents the minimum operating voltage allowed when the converter is connected in parallel. P_{maxi} represents the maximum power that the converter can output, while P_i represents the actual power output during steady-state operation.

The output active power P_0 of the energy storage converter is obtained after passing through the low-pass filter (LPF) to get the output active power P_i, and the reference value V_i^* of the output voltage of the energy storage converter can be obtained by bringing P_i into (5).

$$P_0 = i_{ESS} \times u_{ESS} \tag{6}$$

2) SOC-I DROP CONTROL

During the discharge process, the P-V droop control scheme is utilized for voltage outer loop control in the energy

storage converter, aiming to stabilize the DC bus voltage. Simultaneously, the SOC-I droop control is incorporated into the current inner loop to achieve SOC state equalization for the energy storage unit during the discharge process. The SOC-I droop control is expressed in (7).

$$\Delta I_i = n \bullet (SOC_i - \overline{SOC}) \tag{7}$$

where SOC_i is the state of charge value of each energy storage battery, $\overline{SOC}$ is the average state of charge of all online energy storage batteries, and n is the proportional coefficient.

When the system is initially started, each storage battery begins with a different state. During this period, SOC detection for the storage batteries takes place by comparing their SOC with the average value. If the value of I_i is not equal to zero, indicating an imbalance in the SOC states of the storage batteries, the current inner loop is activated. The calculated difference is then incorporated into the current inner loop, regulating the discharge current through control of the current loop. This action is taken to mitigate SOC imbalances among the energy storage converters.

C. OFF-GRID CONTROL OF POWER SUPPLY CONVERTER

In off-grid mode, the supply converter can be categorized into parallel operation and stand-alone operation.

1) PARALLEL OPERATION DROOP CONTROL

When two power supply converters are operated in parallel, there are output voltage amplitude and frequency deviations between the power supply converters, which need to be regulated by P-F and Q-V droop control, and the droop control for off-grid parallel operation is shown in Fig. 8.

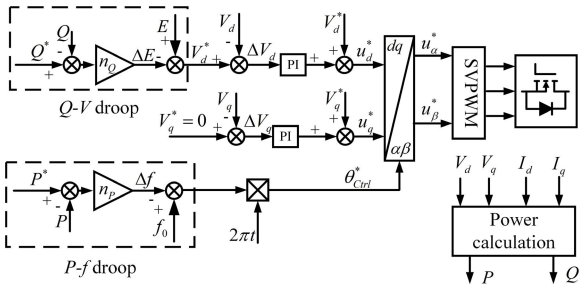

FIGURE 8. Droop control for off-grid parallel operation of the supply converter.

The operation control of the shipboard DC micro-grid power converter is based on vector control, and the output voltage $v_{a,b,c}$ in the natural coordinate system of the power supply converter is Clark-Park transformed to obtain the output voltages in the synchronous rotating d-q coordinate system, V_d, V_q. Similarly, the output currents $i_{a,b,c}$ of the converter are decoupled to obtain the d-axis output current I_d and the q-axis output current I_q. From V_d, V_q, I_d, I_q, the output reactive power measurement Q and active power measurement P of the converter are calculated. Q and P are adjusted to determine the reference value of the output voltage amplitude of the converter, V_d^*, and the frequency reference value, f^*. The V_d^* and f^* are input to the converter by generating the modulating signal SVPWM through the control signal formation link to realize the regulation of voltage magnitude and frequency. The core equation of the droop control of the supply converter is shown in (8).

$$\begin{aligned} f^* &= f_0 - m_P(P^* - P) \\ V_d^* &= E - n_Q(Q^* - Q) \end{aligned} \tag{8}$$

where E, f_0 are the rated output voltage magnitude and frequency of the converter respectively. Q^*, P^* are the rated reference values of reactive and active power output from the converter respectively. m_P, n_Q are the active and reactive droop gains respectively.

2) INDEPENDENT OPERATION OF CONSTANT VOLTAGE/FREQUENCY CONTROL

Constant voltage/frequency control is used when a supply converter operates independently. The purpose of V/F control is to keep the voltage magnitude and frequency of the bus connected to the supply converter constant regardless of the load changes in the system. V/F control maintains the frequency at a given reference value f^* by adjusting the converter output active power measurement P, and the voltage at a given reference value V_d^* by adjusting the output reactive power measurement Q. The core equation for constant voltage/frequency control of the supply converter is shown in (9).

$$\begin{aligned} P^* &= (k_{Pf} + \frac{k_{If}}{s})(f^* - f_0) \\ Q^* &= (k_{Pu} + \frac{k_{Iu}}{s})(V_d^* - E) \end{aligned} \tag{9}$$

where $k_{Pf}, k_{If}, k_{Pu}, k_{Iu}$ are the constant voltage/frequency control parameters of the PI controller.

D. GRID-CONNECTED CONTROL OF POWER SUPPLY CONVERTER

Grid-connected mode means that the port or starboard power supply converter alone operates in parallel with the shore power, and the grid-connected control block diagram is shown in Fig.9.

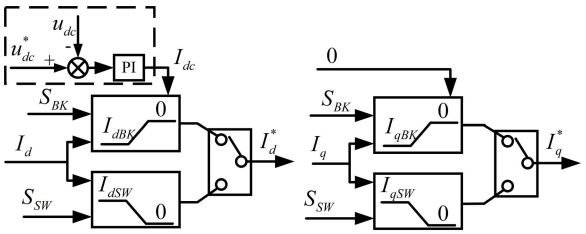

FIGURE 9. Grid-connected control block diagram of the supply converter.

According to the power transfer command S_{SW}, the converter output current value before the switching moment

is locked as the initial value of the output current reference for power transfer, I_{dSW}, and I_{qSW}, and then the closed-loop control of grid-connecting current is adopted. d-q synchronous coordinate system of the grid-connecting current final reference command is recorded as I_d^* and I_q^*. The operation modes of the power converter after the grid connection can be divided into two types: when the charging of the storage battery is completed, or no charging is required, the power converter can directly transfer the power to the shore power and then quit the operation. Adopting single closed-loop control of grid-connected current, the current command will be tapered to 0 ($I_d^* = 0$, $I_q^* = 0$) at a certain slope to complete the power unloading. When the energy storage battery needs to be charged, the power supply converter can be used as a rectifier to stabilize the DC bus voltage and provide power for the charging of the energy storage battery, adopting the double closed-loop control of DC voltage outer loop and grid-connected current inner loop. The active current command is obtained from the intermediate DC bus voltage closed-loop PI controller link, and the reactive current command is tapered to 0. Specifically as shown in (10).

$$\begin{aligned} I_d^* &= (k_{pdc} + \frac{k_{idc}}{s})(u_{dc}^* - u_{dc}) \\ I_q^* &= 0 \end{aligned} \tag{10}$$

where u_{dc}^* is the reference value of DC bus voltage; k_{pdc} and k_{idc} are the proportional and integral coefficients of the PI controller respectively.

To avoid the current impact before and after grid connection, the current slow start link as shown in (11) is added so that the current command gradually transitions from I_{dSW}, I_{qSW} to I_d^*, I_q^*, respectively.

$$\begin{aligned} I_d^* &= I_{dSW} + \int_0^T \Delta i_d dt \\ I_q^* &= I_{qSW} + \int_0^T \Delta i_q dt \end{aligned} \tag{11}$$

where T is the slow start time from the initial to the final value. Δi_d, Δi_q are the current tapering steps. $\Delta i_d = (I_d^* - I_{dSW})/T$, $\Delta i_q = (I_q^* - I_{qSW})/T$.

E. PRE-SYNCHRONIZED CONTROL OF POWER SUPPLY CONVERTER

Pre-synchronization mode refers to adjusting the output voltage of the supply converter to synchronize it with the shore power before grid connection to avoid the voltage shock at the moment of grid connection, and pre-synchronization adopts amplitude and phase synchronization control. The control block diagram is shown in Fig.10.

The output voltages V_d and V_q after decoupling of the converter voltage $V_{a,b,c}$ are phase-locked by the phase-locked loop (PLL) to obtain the converter phase θ_{Con}. Similarly, decoupling of the shore power voltage $V_{g(a,b,c)}$ yields $V_{d-shore}$ and $V_{q-shore}$, and phase-locking yields the

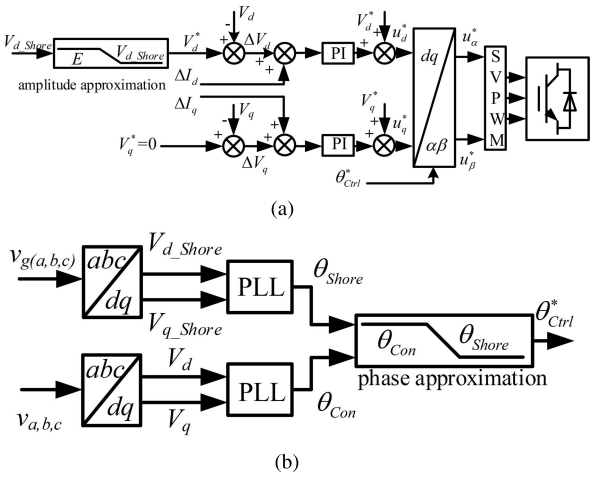

FIGURE 10. Pre-synchronization control of the supply converter. (a) Amplitude pre-synchronization. (b) Phase pre-synchronization.

shore power phase θ_{shore}. The phase approximation unit makes the converter phase θ_{Con} infinitely close to the shore power phase θ_{shore}, and the phase approximation principle is shown in (12).

$$\theta_{Ctrl}^* = \theta_{Con} + \frac{k_\theta}{s}(\theta_{shore} - \theta_{Con}) \tag{12}$$

where k_θ is the integration factor for phase approximation.

Magnitude pre-synchronized acquisition of shore power voltage decoupling to obtain $V_{d-shore}$, $V_{q-shore}$, through the magnitude approximation unit to calculate the power supply converter d-axis output voltage reference value V_d^*, the q-axis output voltage reference value V_q^* is set to 0. The principle of magnitude approximation is shown in the (13).

$$V_d^* = E + \frac{k_E}{s}(V_{d-shore} - E) \tag{13}$$

where k_E is the integral coefficient of the voltage amplitude approximation.

F. SUPPLY CONVERTER VOLTAGE HARMONIC SUPPRESSION

1) ROGI CONTROL PRINCIPLE

Since the output voltage of the generator contains harmonic components and unbalanced components, this paper uses multiple reduced-order generalized integrator (ROGI) to separate and extract the harmonic components and unbalanced components. In this article, the main purpose is to suppress the unbalanced component of the output voltage and typical harmonics such as the 5*th* and 7*th* harmonics. Fig. 11. is the frequency characteristic curve of ROGI, and its transfer function in the s domain is:

$$G_R(s) = \frac{k_i}{s - j\omega_h} \tag{14}$$

where j is the imaginary number sign, k_i is the resonance gain coefficient of ROGI in the s domain, and ω_h is the resonance angular frequency.

$$\omega_h = h\omega_g \tag{15}$$

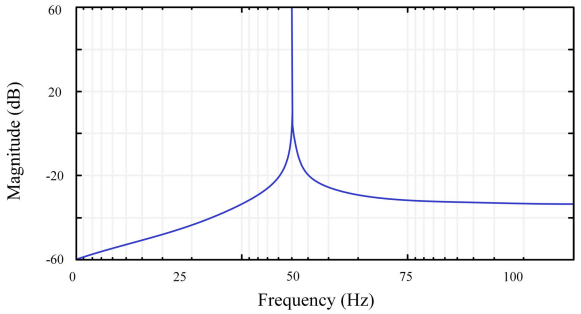

FIGURE 11. ROGI frequency characteristic curve.

where ω_g is the fundamental angular frequency, and h is the harmonic order.

The frequency selection characteristics of ROGI are shown in Fig. 11. It can be observed that the amplitude gain within a certain bandwidth range around the resonant frequency is much higher than the amplitude gain at other frequencies and can be used to track specific frequency signals. However, the gain of ROGI at the resonant frequency is infinite. If it is used directly as a resonant controller, it will destroy the stability of the system. Therefore, in the design process of this article, the cutoff frequency ω_c is added to ROGI to improve the anti-interference ability of the system.

The frequency characteristic curves of the improved ROGI under different k_i and ω_h are shown in Fig. 12. Compared with before the improvement, the gain of the increased ROGI at the resonant frequency is set to a limited value.

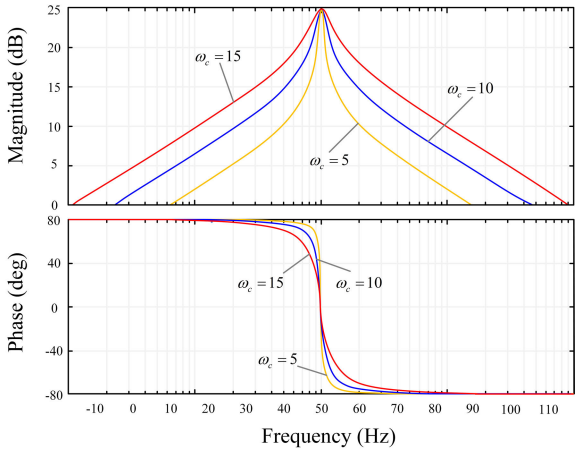

FIGURE 12. Improved frequency characteristic curve.

The improved transfer function is

$$G_R(s) = \frac{k_i \omega_c}{s - j\omega_h + \omega_c} \tag{16}$$

2) ROGI DIGITAL REALIZATION

Since the control algorithm is implemented by a digital signal processor (DSP), the s-domain controller needs to be discretized into the z-domain. However, the commonly used zero-order holding or bilinear transformation discrete methods will cause frequency offset or performance deviation, so this article chooses to directly design the controller parameters in the discrete domain. The pole of the ROGI transfer function is $s_p = jh\omega_h - \omega_c$, which is mapped to the z domain and is $z_p = e^{(-jh\omega_h+\omega_c)T_s}$. The denominator of the ROGI transfer function is:

$$D_R(z) = z - e^{jh\omega_h T_s} e^{-\omega_c T_s} \tag{17}$$

where T_s is the sampling period. As the controlled object, the transfer function of the PWM controller can be expressed as:

$$G(s) = \frac{\omega_n^2}{s^2 + 2\xi\omega_n s + \omega_n^2} = \frac{\omega_n^2}{(s - \omega_{n1})(s - \omega_{n2})} \tag{18}$$

There are two poles of $s_{p1} = \omega_{n1}$, $s_{p2} = \omega_{n2}$ in the controlled object, which are mapped to $z_{p1} = e^{\omega_{n1} T_s}$, $z_{p2} = e^{\omega_{n2} T_s}$ in the z domain. It can be deduced that the transfer function of ROGI of $h-th$ harmonic in the z domain is:

$$G_R(z) = \frac{k_h(z+1)}{z - e^{jh\omega_g T_s} + e^{-\omega_c T_s}} \tag{19}$$

where k_h is the resonance coefficient of ROGI of the $h-th$ harmonic in the z domain.

The transfer function of ROGI has complex factors which are not conducive to the digital implementation of the controller, so ROGI needs to be applied in the $\alpha - \beta$ coordinate system. Because the variables in the $\alpha - \beta$ coordinate system have the characteristics of $x_\alpha = jx_\beta$, combined with Euler's formula $e^{jx} = cosx + jsinx$, the digital implementation of ROGI can be obtained, as shown in Fig. 13.

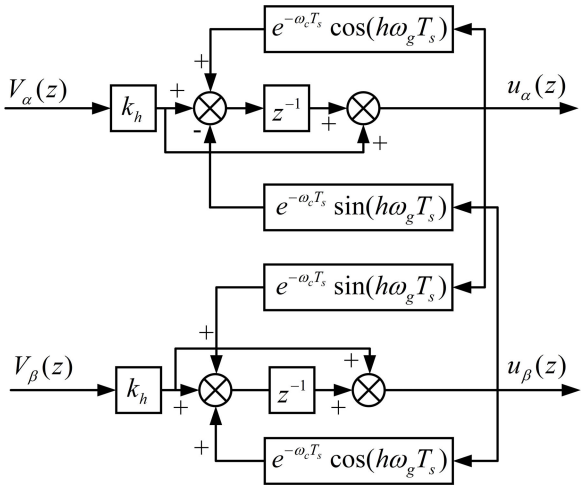

FIGURE 13. ROGI digital implementation block diagram.

where $V_\alpha(z)$ and $V_\beta(z)$ are respectively the expressions of u_α, u_β in the z domain, and $u_\alpha(z)$, $u_\beta(z)$ are respectively the z domain expressions of the $\alpha - \beta$ axis component of the ROGI output.

According to the digital implementation process of ROGI, the differential equation of ROGI for the $h-th$ harmonic can

be obtained.

$$\begin{aligned} u_{\alpha h}(k) &= K_h[V_\alpha(k) + V_\alpha(k-1)] + mu_{\alpha h}(k-1) \\ &\quad + nu_{\beta h}(k-1) \\ u_{\beta h}(k) &= K_h[V_\beta(k) + V_\beta(k-1)] + mu_{\beta h}(k-1) \\ &\quad + nu_{\alpha h}(k-1) \\ m &= e^{-\omega_c T_s} cos(h\omega_1 T_s) \end{aligned} \tag{20}$$

According to the difference equation, the superposition of the allowable inhibition amounts of multiple ROGI can be obtained.

$$\begin{aligned} \sum u_{\alpha h}(k) &= \sum_{h=-2,-5,-7} u_{\alpha h}(k) \\ \sum u_{\beta h}(k) &= \sum_{h=-2,-5,-7} u_{\beta h}(k) \end{aligned} \tag{21}$$

where $u_{\alpha h}(k)$ and $u_{\beta h}(k)$ are, respectively, the $\alpha - \beta$ axis superposition amount of the required suppression amount in the α, β coordinate system.

IV. EXPERIMENTAL VALIDATION

To verify the feasibility of the proposed converter control method, an experimental platform for shipboard DC micro-grid system is built as shown in Fig. 14, and its main parameters are shown in Table 1.

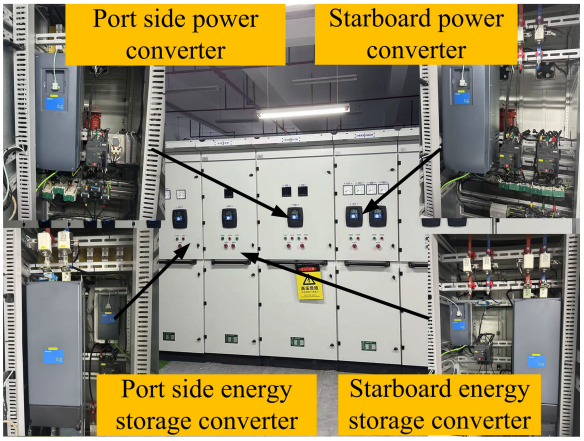

FIGURE 14. Shipboard DC micro-grid experimental platform.

A. ENERGY STORAGE CONVERTER CHARGING AND DISCHARGING EXPERIMENTAL RESULTS

The result of the energy storage converter charging process is depicted in Fig. 15. The energy storage converter remains inactive until $t < 0.1h$ and is not engaged until $t = 0.1h$. In the initial charging phase, the current loop is activated for constant-current charging, with a single-phase charging current of approximately 500A. The terminal voltage of the energy storage battery exhibits a linear rising trend. By $t = 0.9h$, the terminal voltage reaches the preset value of 480V. At this point, the voltage outer loop is activated for

TABLE 1. Main parameters of the converter.

Main parameters	Value
DC bus-rated voltage	1050V
DC bus support capacitor	10mF
Battery Voltage	800V
Battery Rated Capacity	300kWh
Single filter inductor	0.5mH
switch frequency	2.5kHz
Power level	750kVA
Frequency	50Hz
Voltage Harmonic Content	<5%
Voltage unbalance	<2%
Shock load resistant	180kVA

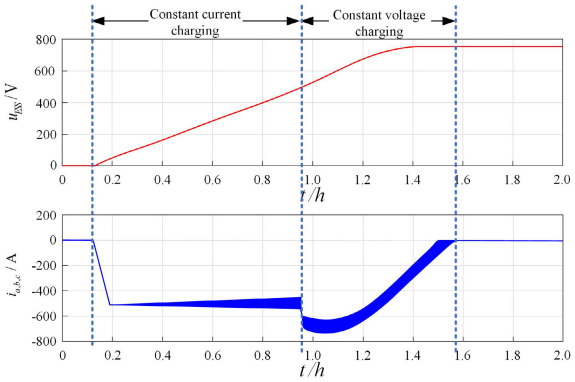

FIGURE 15. Experimental results of energy storage converter charging.

constant voltage charging, leading to a gradual decrease in the charging current until the charging process is complete.

The result of the discharge process of the energy storage converter is shown in Fig. 16. When $t < 0.1h$, the energy storage converter is not activated, and at $t = 0.1h$, the converter is put into operation. The DC bus voltage starts to rise and is affected by the disturbance at the early stage

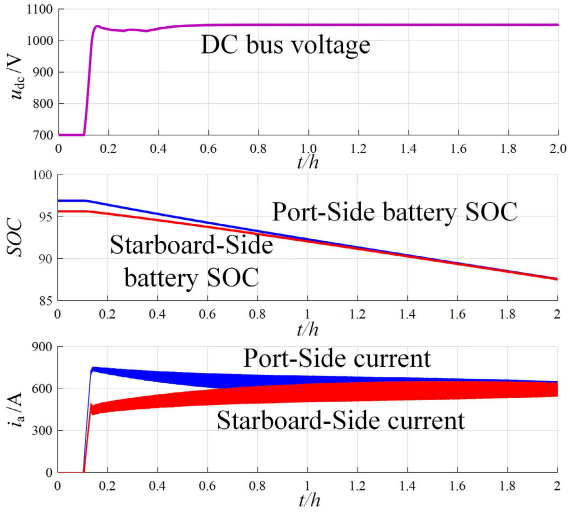

FIGURE 16. Experimental results of energy storage converter discharge.

of the discharge, and the DC bus voltage fails to stabilize at 1050 V. The P-V droop control comes into play to stabilize the DC bus voltage problem by distributing the power output proportionally according to the different capacities of the port side converter and the starboard side converter. After 0.5h, the DC bus voltage is basically maintained at 1050 V after the P-V droop control.

Meanwhile, in the initial stage of discharge, the initial state of the SOC of the port side storage battery and the SOC of the starboard side storage battery are different. The SOC-I droop control added in the current loop can regulate the output power of the port and starboard storage batteries according to the state of the SOC on the premise that the DC bus voltage is stabilized. The SOC of the port and starboard storage batteries are gradually balanced, so that the output power of the port converter and starboard converter is equalized.

The SOC change results of charging and discharging the energy storage battery are shown in Fig 17.

The result of the charging experiment is shown in Fig. 17(a). At the initial moment of charging, the SOC of the starboard battery is lower than the SOC of the port battery, so the slope of the SOC of the starboard battery is more jittery and rises faster than the decrease of the SOC of the port battery. Finally the SOC of the two sides of the battery gradually tends to equalize.

The result of the discharge experiment is shown in Fig. 17(b). At the initial discharge moment, the SOC of the port battery is larger than that of the starboard battery, so the slope of the SOC of the port battery is more jittery and decreases faster than the SOC of the starboard battery. Finally the SOC of the two batteries gradually equalizes.

The result of charging and discharging is shown in Fig. 17(c). At the beginning stage, the energy provided by the shipboard DC micro-grid is not enough to meet the load's demand, so the storage battery works in the discharging state, and the initial value of the port battery SOC is larger than that of the starboard battery SOC, so the decrease of the port battery SOC is faster. At $t = 22min$, the energy provided by the shipboard DC micro-grid exceeds the load's demand, and the storage battery switches to the charging state, and the port battery SOC is larger than the starboard battery SOC, so the starboard battery SOC rises faster. At $t = 40min$, the energy provided by the shipboard DC micro-grid is not enough to meet the load demand, the energy storage battery work again switches to the discharge state. Under the charging and discharging mode switching, the SOC of the two sides of the battery gradually tends to balance. Compared with [12], the P-V and SOC-I double-drop control strategy proposed in this paper is more advantageous in terms of SOC state equalization of the energy storage system as well as bus voltage stabilization.

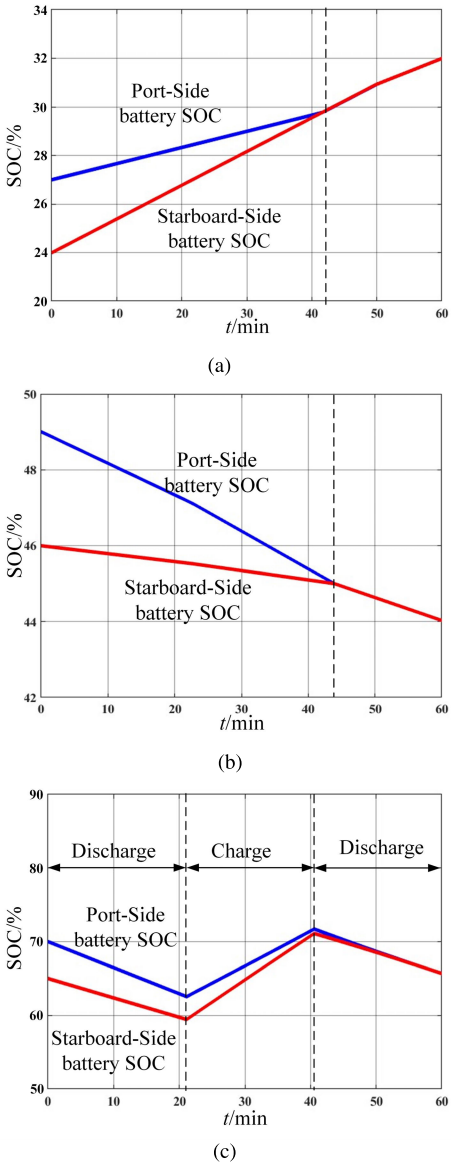

FIGURE 17. Results of battery charging and discharging SOC changes. (a) charge SOC. (b) discharge SOC. (c) charge and discharge SOC.

B. POWER SUPPLY CONVERTER ON/OFF-GRID EXPERIMENTAL RESULTS

Fig. 18 shows the experimental results of the power converter and shore power on/off-grid process. The figure shows the A-phase grid-connected voltage as well as the three-phase current, v_a indicates the supply converter voltage, and v_{ga} indicates the shore power grid voltage. The off-grid control of the power supply converter with or without load is performed with shore power, respectively.

In Fig. 18(a), the power converter is connected to the shore power at the time of t_1 under load conditions and switches to the current control mode to unload the output power to 0 after receiving feedback from the grid-connected state.

In Fig. 18(b), the power converter is off-grid with the shore power at t_2 under load condition and switches back to the AC bus voltage control mode after receiving the feedback of off-grid status, and there is no obvious voltage drop or oscillation of AC bus voltage during the off-grid process.

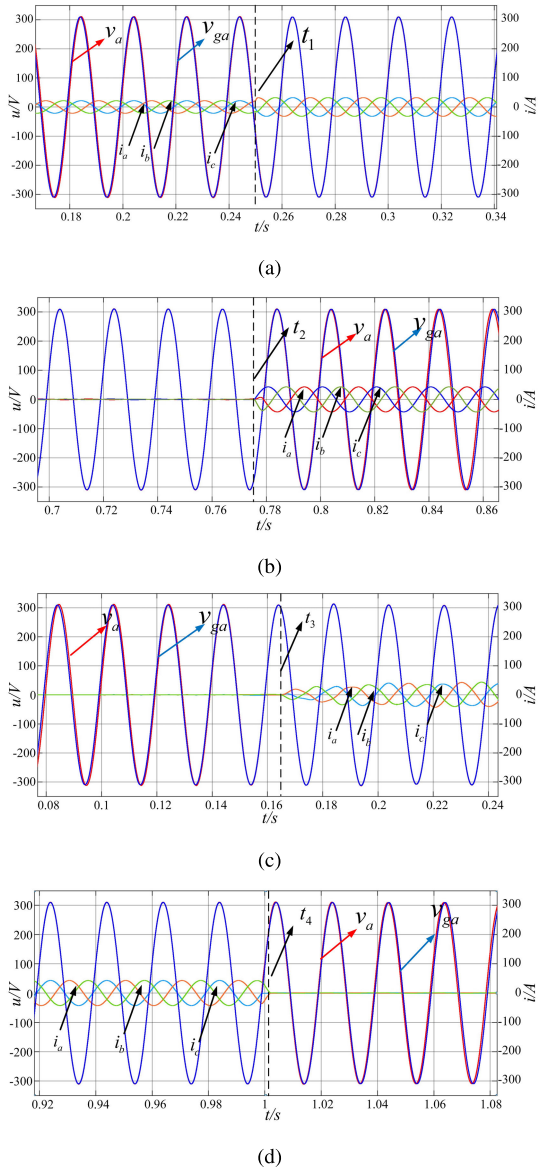

FIGURE 18. Results of power supply converter on/off-grid experiments. (a) Grid-connected with load. (b) off-grid with load. (c) no-load grid connection. (d) idle off-grid.

In Fig. 18(c), the power converter is connected to the shore power at t_3 under no-load condition switches to the current control mode after receiving the feedback from the grid-connected state, and enters the power transfer state to unload the output power to zero.

In Fig. 18(d), the power converter is off-grid with shore power at t_4 under no-load condition and switches back to AC bus voltage control mode after receiving feedback from the off-grid state, and there is no obvious voltage drop or oscillation of AC bus voltage during the off-grid process. Compared with [22], the flexible on/off-grid control proposed in this paper has better fast response as well as power transfer characteristics under on/off-grid, especially under different loads.

The results of the pre-synchronized grid-connection experiment is shown in Fig. 19. Phase difference between the output voltage of the power converter and the shore power voltage amplitude before t_5. After the synchronization control is turned on, the amplitude and phase of the output voltage of the power supply converter are constantly approaching the shore power to complete the grid connection.

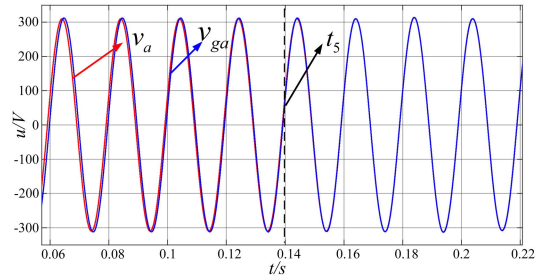

FIGURE 19. Results of pre-synchronization experiments.

The output voltage harmonic suppression results of the power supply converter are shown in Fig. 20.

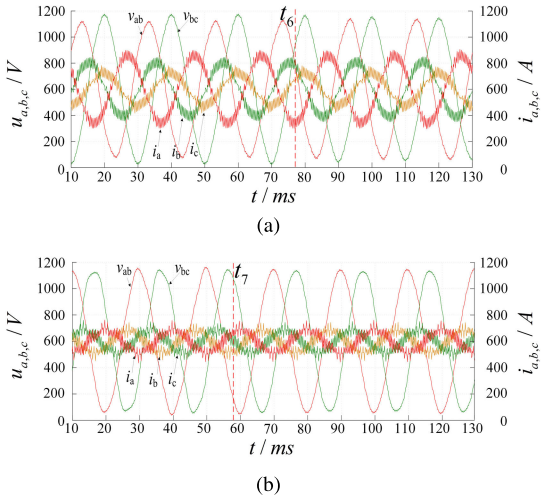

FIGURE 20. Output voltage harmonic suppression experimental results. (a) Unbalance suppression. (b) Harmonic suppression.

Fig. 20(a) shows the output voltage experimental results, and the output voltage of the power supply converter before the moment of t_6 is unbalanced. After adding the voltage unbalance suppression control algorithm, the output voltage is quickly restored to the balanced state, and the voltage unbalance is reduced from 8% to within 1%.

Fig. 20(b) shows the results of the harmonic suppression experiment. Due to the influence of nonlinear devices, more voltage harmonics are generated. After adding the harmonic suppression algorithm at t_7, the output voltage gradually converges to the sinusoidal voltage.

The spectrum analysis of the output voltage is shown in Fig.21. As can be seen from Fig. 21(a), without harmonic voltage compensation, the amplitude of the largest

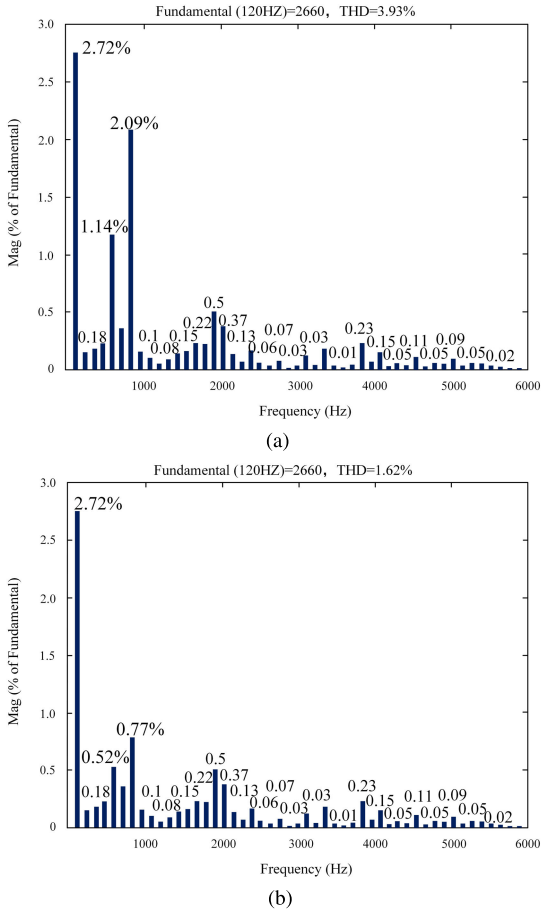

FIGURE 21. Output voltage spectrum analysis. (a) Before inhibition. (b) After inhibition.

waveforms are the 5th and 7th harmonics, which are nearly 1.14% and 2.09%, and the total harmonic suppression rate is 3.93%, and after the 5th and 7th harmonic suppression, as shown in Fig. 21(b), the 5th and 7th harmonic content in the grid voltage decreases to 0.52% and 0.77%, and the total harmonic suppression rate decreases to 1.62%, which meets the requirements of the grid harmonic suppression rate. Influenced by the nonlinear loads and power electronic loads in the ship's power system, high harmonics will be generated, affecting the power quality of the micro-grid. And due to the complex external environment of the shipboard DC micro-grid system, it is easy to have an impact on the amplitude of high harmonics. While in this paper, the content of high harmonics is less than 0.5%, which has less impact on the quality of the micro-grid, so it can be ignored. Compared with [31], the ROGI harmonic suppression proposed in this paper uses a discrete design, which can effectively avoid controller performance bias during the digitization process.

V. CONCLUSION

This proposal focuses on shipboard DC micro-grid system to meet the challenges of its power system stability and reliability. The P-V voltage droop control and SOC-I current control methods are proposed for the energy storage converter, and the charging and discharging control scheme is designed to stabilize the DC bus voltage. In charging control, ''constant current-constant voltage'' control is used in combination with SOC-I current droop control to balance the SOC of the storage battery. While in discharging control, P-V voltage droop control and SOC-I current droop control are used to stabilize the DC bus voltage and ensure the SOC of the battery is balanced, thus realizing output power Equalization. In on/off-grid control, the control method of switching voltage and current control modes is introduced for the power supply converter. When the power supply converter is running off-grid with load, the voltage control mode is adopted to ensure the fast response performance of the output voltage. When the power supply converter is running on-grid, current control is used to ensure precise control of the output current. Meanwhile, different functions such as exit after unloading and rectified power supply to maintain DC bus voltage can be realized according to needs. When switching between different modes, the control mode is quickly switched through the feedback signal of the grid-connected circuit breaker status, and at the same time, the pre-synchronization control and voltage-current control are combined to realize the flexible switching away from the grid to ensure the safe operation of the system. The frequency selection characteristic of ROGI is used to achieve the suppression of output voltage unbalance and typical harmonics such as the 5*th* and 7*th* harmonics.The effectiveness of the proposed control strategy for shipboard converter is verified through experimental validation, which provides the feasibility for the stable operation of shipboard DC micro-grid system. However, the energy storage system in this paper selects a single storage battery as the energy storage device, which stores limited energy. In the harmonic suppression part, considering that the higher harmonics are lower and have less impact on the grid quality, it is only for the 5*th* and 7*th* harmonics.

REFERENCES

[1] S. Fang, Y. Wang, B. Gou, and Y. Xu, ''Toward future green maritime transportation: An overview of seaport microgrids and all-electric ships,'' *IEEE Trans. Veh. Technol.*, vol. 69, no. 1, pp. 207–219, Jan. 2020, doi: 10.1109/TVT.2019.2950538.

[2] L. Xu, J. M. Guerrero, A. Lashab, B. Wei, N. Bazmohammadi, J. C. Vasquez, and A. Abusorrah, ''A review of DC shipboard microgrids—Part I: Power architectures, energy storage, and power converters,'' *IEEE Trans. Power Electron.*, vol. 37, no. 5, pp. 5155–5172, May 2022, doi: 10.1109/TPEL.2021.3128417.

[3] M. A. Hassan, C.-L. Su, J. Pou, G. Sulligoi, D. Almakhles, D. Bosich, and J. M. Guerrero, ''DC shipboard microgrids with constant power loads: A review of advanced nonlinear control strategies and stabilization techniques,'' *IEEE Trans. Smart Grid*, vol. 13, no. 5, pp. 3422–3438, Sep. 2022, doi: 10.1109/TSG.2022.3168267.

[4] T. Morstyn, B. Hredzak, and V. G. Agelidis, ''Control strategies for microgrids with distributed energy storage systems: An overview,'' *IEEE Trans. Smart Grid*, vol. 9, no. 4, pp. 3652–3666, Jul. 2018, doi: 10.1109/TSG.2016.2637958.

[5] M. Mosayebi, S. M. Sadeghzadeh, M. Gheisarnejad, and M. H. Khooban, ''Intelligent and fast model-free sliding mode control for shipboard DC microgrids,'' *IEEE Trans. Transport. Electrific.*, vol. 7, no. 3, pp. 1662–1671, Sep. 2021, doi: 10.1109/TTE.2020.3048552.

[6] M. U. Mutarraf, Y. Terriche, M. Nasir, Y. Guan, C.-L. Su, J. C. Vasquez, and J. M. Guerrero, "A communication-less multimode control approach for adaptive power sharing in ship-based seaport microgrid," *IEEE Trans. Transport. Electrific.*, vol. 7, no. 4, pp. 3070–3082, Dec. 2021, doi: 10.1109/TTE.2021.3087722.

[7] A. Francés-Roger, A. Anvari-Moghaddam, E. Rodríguez-Díaz, J. C. Vasquez, J. M. Guerrero, and J. Uceda, "Dynamic assessment of COTS converters-based DC integrated power systems in electric ships," *IEEE Trans. Ind. Informat.*, vol. 14, no. 12, pp. 5518–5529, Dec. 2018, doi: 10.1109/TII.2018.2810323.

[8] Z. Jin, L. Meng, J. M. Guerrero, and R. Han, "Hierarchical control design for a shipboard power system with DC distribution and energy storage aboard future more-electric ships," *IEEE Trans. Ind. Informat.*, vol. 14, no. 2, pp. 703–714, Feb. 2018, doi: 10.1109/TII.2017.2772343.

[9] S. Faddel, A. A. Saad, T. Youssef, and O. Mohammed, "Decentralized control algorithm for the hybrid energy storage of shipboard power system," *IEEE J. Emerg. Sel. Topics Power Electron.*, vol. 8, no. 1, pp. 720–731, Mar. 2020, doi: 10.1109/JESTPE.2019.2899287.

[10] J. Su, K. Li, Y. Li, C. Xing, and J. Yu, "A novel state-of-charge-based droop control for battery energy storage systems to support coordinated operation of DC microgrids," *IEEE J. Emerg. Sel. Topics Power Electron.*, vol. 11, no. 1, pp. 312–324, Feb. 2023, doi: 10.1109/JESTPE.2022.3149398.

[11] Z. Li, K. W. Chan, J. Hu, and J. M. Guerrero, "Adaptive droop control using adaptive virtual impedance for microgrids with variable PV outputs and load demands," *IEEE Trans. Ind. Electron.*, vol. 68, no. 10, pp. 9630–9640, Oct. 2021, doi: 10.1109/TIE.2020.3022524.

[12] X. Sun, Y. Hao, Q. Wu, X. Guo, and B. Wang, "A multifunctional and wireless droop control for distributed energy storage units in islanded AC microgrid applications," *IEEE Trans. Power Electron.*, vol. 32, no. 1, pp. 736–751, Jan. 2017, doi: 10.1109/TPEL.2016.2531379.

[13] H. Wang, Q. Zhang, D. Wu, and J. Zhang, "Advanced current-droop control for storage converters for fault ride-through enhancement," *IEEE J. Emerg. Sel. Topics Power Electron.*, vol. 8, no. 3, pp. 2461–2474, Sep. 2020, doi: 10.1109/JESTPE.2019.2910587.

[14] S. Sahoo, S. Mishra, S. Jha, and B. Singh, "A cooperative adaptive droop based energy management and optimal voltage regulation scheme for DC microgrids," *IEEE Trans. Ind. Electron.*, vol. 67, no. 4, pp. 2894–2904, Apr. 2020, doi: 10.1109/TIE.2019.2910037.

[15] M. Baharizadeh, M. S. Golsorkhi, M. Shahparasti, and M. Savaghebi, "A two-layer control scheme based on $P - V$ droop characteristic for accurate power sharing and voltage regulation in DC microgrids," *IEEE Trans. Smart Grid*, vol. 12, no. 4, pp. 2776–2787, Jul. 2021, doi: 10.1109/TSG.2021.3060074.

[16] J. Chen, D. Yue, C. Dou, L. Chen, S. Weng, and Y. Li, "A virtual complex impedance based $P - \dot{V}$ droop method for parallel-connected inverters in low-voltage AC microgrids," *IEEE Trans. Ind. Informat.*, vol. 17, no. 3, pp. 1763–1773, Mar. 2021, doi: 10.1109/TII.2020.2997054.

[17] D. Xu, A. Xu, C. Yang, and P. Shi, "A novel double-quadrant SoC consistent adaptive droop control in DC microgrids," *IEEE Trans. Circuits Syst. II, Exp. Briefs*, vol. 67, no. 10, pp. 2034–2038, Oct. 2020, doi: 10.1109/TCSII.2019.2945009.

[18] Q. Wu, R. Guan, X. Sun, Y. Wang, and X. Li, "SoC balancing strategy for multiple energy storage units with different capacities in islanded microgrids based on droop control," *IEEE J. Emerg. Sel. Topics Power Electron.*, vol. 6, no. 4, pp. 1932–1941, Dec. 2018, doi: 10.1109/JESTPE.2018.2789481.

[19] T. A. Fagundes, G. H. F. Fuzato, C. R. De Aguiar, K. D. A. Ottoboni, M. Biczkowski, and R. Q. Machado, "Management and equalization of energy storage devices for DC microgrids using a SoC-sharing function," *IEEE Access*, vol. 8, pp. 78576–78589, 2020, doi: 10.1109/ACCESS.2020.2990191.

[20] K. Bi, W. Yang, D. Xu, and W. Yan, "Dynamic SOC balance strategy for modular energy storage system based on adaptive droop control," *IEEE Access*, vol. 8, pp. 41418–41431, 2020, doi: 10.1109/ACCESS.2020.2976729.

[21] M. Rezkallah, F. Dubuisson, S. Singh, B. Singh, A. Chandra, H. Ibrahim, and M. Ghandour, "Coordinated control strategy for hybrid off-grid system based on variable speed diesel generator," *IEEE Trans. Ind. Appl.*, vol. 58, no. 4, pp. 4411–4423, Jul. 2022, doi: 10.1109/TIA.2022.3174825.

[22] A. C. Sunny and D. Debnath, "A novel low device count four-port converter based solar-fed off-grid system for catering household hybrid AC/DC loads," *IEEE Trans. Power Electron.*, vol. 38, no. 2, pp. 2658–2667, Feb. 2023, doi: 10.1109/TPEL.2022.3213991.

[23] B. Housseini, A. F. Okou, and R. Beguenane, "Robust nonlinear controller design for on-grid/off-grid wind energy battery-storage system," *IEEE Trans. Smart Grid*, vol. 9, no. 6, pp. 5588–5598, Nov. 2018, doi: 10.1109/TSG.2017.2691707.

[24] T. Liu, P. Wang, J. Ma, R. Zhang, S. Wang, Z. Wu, and R. Wang, "Presynchronization control for grid-connected inverters without grid voltage sensors," *IEEE Trans. Power Electron.*, vol. 38, no. 3, pp. 2833–2838, Mar. 2023, doi: 10.1109/TPEL.2022.3221072.

[25] H. R. Baghaee, M. Mirsalim, G. B. Gharehpetian, and H. A. Talebi, "Decentralized sliding mode control of WG/PV/FC microgrids under unbalanced and nonlinear load conditions for on- and off-grid modes," *IEEE Syst. J.*, vol. 12, no. 4, pp. 3108–3119, Dec. 2018, doi: 10.1109/JSYST.2017.2761792.

[26] R.-J. Wai, Q.-Q. Zhang, and Y. Wang, "A novel voltage stabilization and power sharing control method based on virtual complex impedance for an off-grid microgrid," *IEEE Trans. Power Electron.*, vol. 34, no. 2, pp. 1863–1880, Feb. 2019, doi: 10.1109/TPEL.2018.2831673.

[27] J. Wang, N. Ramli, and N. H. A. Aziz, "Pre synchronization control strategy of virtual synchronous generator (VSG) in micro-grid," *IEEE Access*, vol. 11, pp. 139004–139016, 2023, doi: 10.1109/ACCESS.2023.3341102.

[28] Q. Chen, "A control strategy of islanded microgrid with nonlinear load for harmonic suppression," *IEEE Access*, vol. 9, pp. 39171–39181, 2021, doi: 10.1109/ACCESS.2021.3064413.

[29] G. Lou, Q. Yang, W. Gu, X. Quan, J. M. Guerrero, and S. Li, "Analysis and design of hybrid harmonic suppression scheme for VSG considering nonlinear loads and distorted grid," *IEEE Trans. Energy Convers.*, vol. 36, no. 4, pp. 3096–3107, Dec. 2021, doi: 10.1109/TEC.2021.3063607.

[30] B. Pang, X. Zhu, J. Yang, K. Liao, B. Chen, and Z. He, "Voltage harmonics optimization for weak grid-tied doubly-fed induction generator with the capability of suppressing current harmonics," *IEEE Trans. Energy Convers.*, vol. 38, no. 2, pp. 1452–1460, Jun. 2023, doi: 10.1109/TEC.2022.3233843.

[31] S. Yin and X. Wang, "A novel current harmonic suppression method for HSPMSG based on the hybrid rectifier," *IEEE Trans. Transport. Electrific.*, vol. 9, no. 3, pp. 4594–4604, Sep. 2023, doi: 10.1109/TTE.2023.3243023.

[32] Z. Li, Z. Yu, W. Kong, R. Qu, and D. Li, "An accurate harmonic current suppression strategy for DC-biased Vernier reluctance machines based on adaptive notch filter," *IEEE Trans. Ind. Electron.*, vol. 69, no. 5, pp. 4555–4565, May 2022, doi: 10.1109/TIE.2021.3078400.

[33] W. Yang, M. Wang, S. Aziz, and A. Y. Kharal, "Magnitude-reshaping strategy for harmonic suppression of VSG-based inverter under weak grid," *IEEE Access*, vol. 8, pp. 184399–184413, 2020, doi: 10.1109/ACCESS.2020.3026054.

XUN CHEN (Member, IEEE) received the B.E. degree in automation from the East China Shipbuilding Institute, in 1998, the M.E. degree in control theory and control engineering from Nanjing University of Science and Technology, in 2004, and the Ph.D. degree in computer system architecture from Fudan University, in 2008.

He is currently an Associate Professor with Jiangsu University of Science and Technology. His research interests include intelligent detection technology and devices, embedded systems, and power electronic technology.

RUI TIAN (Student Member, IEEE) was born in Lianyungang, China, in 2000. He received the bachelor's degree in engineering from Jiangsu University of Science and Technology, China, in 2022, where he is currently pursuing the master's degree. His active research interest includes shipboard DC micro-grid systems.

SONG XU (Member, IEEE) was born in Zhenjiang, China, in 1991. He received the B.S. and M.S. degrees (Hons.) from the College of Electrical, Energy and Power Engineering, Yangzhou University, Yangzhou, China, in 2014 and 2017, respectively, and the Ph.D. degree from the Division of Electronics and Informatics, College of Science and Technology, Gunma University, Kiryu, Gunma, Japan, in 2020.

From March 2020 to October 2020, he was a Foreign Researcher with Gunma University. In 2020, he joined Jiangsu University of Science and Technology, where he is currently a Lecturer with the College of Automation. His current research interests include big data compression, digitalized power transfer to renewable energy and energy storage devices, and intelligent control applications in industrial processes.

Dr. Xu's awards and honors include the three times "Best Presentation Award" of International Conference ICMEMIS, in 2017, 2018, and 2019, respectively. The Second Prize of Yangzhou Natural Science Outstanding Paper Award and Second Prize of Science and Technology Progress Award of Jiangsu Cold Chain Society.

WEI JIANG (Member, IEEE) was born in Yangzhou, China, in 1980. He received the B.S.E.E. degree from Southwest Jiaotong University, Chengdu, China, in 2003, and the M.Sc. and Ph.D. degrees in electrical engineering from The University of Texas at Arlington, TX, USA, in 2006 and 2009, respectively.

From 2007 to 2008, he was a Senior Design Engineer with EF Technologies LLC, TX, USA. In 2010, he joined Yangzhou University and founded the Smart Energy Laboratory, where he is currently a Professor. He has been a Visiting Professor with Gunma University, Japan, in 2012, University of Strathclyde, and Aston University, U.K., in 2015. He holds two U.S. patents and 15 Chinese patents with two licensed by the industry. His current research interests include digitalized power conditioning to renewable energy and energy storage devices and microscopic analysis of electromechanical energy conversion.

Dr. Jiang was the four-time Yangzhou University Excellent Teaching Award Winner.

YONGHONG WANG (Student Member, IEEE) was born in Baoji, China, in 1974. He received the Graduate degree in mechatronics engineering from Nanjing University of Technology.

He is currently a Senior Lecturer in electrical and a Senior Technician in maintenance electrician. He has presided over and participated in six national, provincial and municipal projects, published five textbooks, nine articles, six authorized patents, 11 registered computer software copyrights, and 13 teaching awards. His main research interests include intelligent control technology, mechatronics system integration, and the integration of information technology and education and teaching. He is also an Expert of the Teaching Steering Committee of the National Highly Skilled Personnel Training Base Construction Project, a member of the Teaching Innovation Working Committee of Chinese Society for Vocational and Technical Education, a Teacher Training Expert of Secondary Vocational Schools in Guangdong Province, a Leading Teacher of Automation Control in Guangzhou, an Excellent Teacher in Guangzhou, and a Backbone Teacher of Science and Technology Education for Young People in Guangzhou.

SEIJI HASHIMOTO (Member, IEEE) was born in Aomori, Japan, in 1971. He received the M.E. and Ph.D. degrees in electrical and electronic engineering from Utsunomiya University, Japan, in 1996 and 1999, respectively.

He joined the Department of Mechanical Engineering, Oyama National College of Technology. Since 2002, he has been a Research Associate with the Department of Electronic Engineering, Gunma University, where he is currently a Professor with the Division of Electronics and Informatics. He has consulted for companies in control and energy applications and been a Visitor Professor in China. His research interests include system identification, motion control, and intelligent control and its application to industrial fields.